

Phase analysis, thermal and thermoelectric properties of nanocrystalline $\text{Na}_{0.15}\text{Cu}_{1.85}\text{S}$, $\text{Na}_{0.17}\text{Cu}_{1.80}\text{S}$, $\text{Na}_{0.20}\text{Cu}_{1.77}\text{S}$ alloys

M.Kh. Balapanov^{*,1}, M.M. Kubenova², K.A. Kuterbekov²,
A. Kozlovskiy², S.N. Nurakov², R.Kh. Ishembetov¹,
R.A. Yakshibaev¹

¹Bashkir State University, Ufa, Russia

²L.N.Gumilyov Eurasian National University, Astana, Kazakhstan

E-mail: balapanovmk@mail.ru

DOI: 10.29317/ejpfm.2018020304

Received: 03.09.2018

Synthesis, X-ray phase analysis, electron microscopy and investigations of the thermoelectric and thermal properties of nanocrystalline copper sulfide alloys contained sodium are presented. At room temperature, the alloys are a mixture of three phases of copper sulfide - the monoclinic phase of $\text{Na}_2\text{Cu}_4\text{S}_3$, the hexagonal phase of Cu_2S and the cubic phase of Cu_9S_5 (digenite). The predominant phase is $\text{Na}_2\text{Cu}_4\text{S}_3$ (with content from 57 to 85 volume %). The particle sizes in the compacted samples lie in the range from 20 to 400 nm. For all samples DSC studies revealed a first-order phase transition in the (370-380) K region with enthalpies from 5234 to 11720 J/kgK. The heat capacity varies within the range (0.15-0.48) J/(gK). The electrical conductivity, Seebeck coefficient and thermal conductivity were measured in the temperature range from 290 to 590 K. A very low thermal conductivity of the samples was observed in the interval of (0.1-0.6) $\text{Wm}^{-1}\text{K}^{-1}$. The Seebeck coefficient has a value higher than 0.2 mV/K for $\text{Na}_{0.15}\text{Cu}_{1.85}\text{S}$ composition, but a low electrical conductivity about 10 S/cm limits the maximum dimensionless thermoelectric efficiency ZT of the material at 0.3 in the temperature range 290-590 K.

Keywords: copper sulfide, thermal conductivity, thermoelectric materials, superionic conductors.

Introduction

Copper sulfides have interesting physical properties for using in solar cells, thermoelectric generators, optical filters, solid-state ionic devices and other structures [1-3]. A wide range of homogeneity of copper sulphide in the metal sublattice (from Cu_2S to $\text{Cu}_{1.75}\text{S}$) favors to strong doping with other metals without changes in the crystal structure type [4], which makes it possible to synthesize homogeneous samples with the desired useful properties.

In the literature, there are reports that in quasi-binary systems with heavy alkaline cations (such as $\text{Cu}_2\text{S-K}_2\text{S}$, $\text{Cu}_2\text{S-Rb}_2\text{S}$, $\text{Cu}_2\text{S-Tl}_2\text{S}$), disproportionated quasi-one-dimensional structures with the general formula ACu_7S_4 (A = Tl, K, Rb) [5] are formed, which is equivalent to formula $\text{A}_{0.25}\text{Cu}_{1.75}\text{S}$. In paper [6], the authors used the DSC method to study the transition of $\text{K}_{0.1}\text{Cu}_{1.9}\text{S}$ into a superionic state, and determined the specific heat of the phase transition, equal to 5.5 mJ/g^{-1} . The phase transition started at 366 K and ended at 375 K. The transition temperature corresponds to the phase transition from the low-temperature monoclinic (or orthorhombic [7,8]) phase of copper sulfide to a medium-temperature hexagonal modification with high ionic conductivity [9]. It is known a quasi-one-dimensional $\text{Na}_2\text{Cu}_4\text{S}_3$ compound exists [10]. However, at low sodium concentrations, the crystal structure of copper sulfide does not change [11]. The authors of [11] obtained homogeneous $\text{Na}_x\text{Cu}_9\text{S}_5$ samples at $x=0.025$, 0.05 and 0.15 with a maximum thermoelectric figure merit $ZT = 1.1$ at 773 K for the composition $x=0.05$ (in our terminology $x=0.05$ corresponds to the composition $\text{Na}_{0.01}\text{Cu}_{1.80}\text{S}$).

In our recent paper [12], we synthesized and investigated the electronic and ionic transport of stoichiometric $\text{Na}_x\text{Cu}_{2-x}\text{S}$ ($x=0.05$; 0.1; 0.15; 0.2) compositions, which may be of interest as promising thermoelectric materials. In this paper, we synthesized $\text{Na}_{0.15}\text{Cu}_{1.85}\text{S}$, $\text{Na}_{0.17}\text{Cu}_{1.80}\text{S}$ and $\text{Na}_{0.20}\text{Cu}_{1.77}\text{S}$ compositions, and carried out the investigations of the obtained phases by X-ray diffractometry, electron microscopy and energy dispersive X-ray spectral analysis, and also had measured thermoelectric and thermal properties in the region (290-590) K to estimate the prospects of their use as thermoelectric materials.

Experimental

Samples of compositions $\text{Na}_{0.15}\text{Cu}_{1.85}\text{S}$, $\text{Na}_{0.17}\text{Cu}_{1.80}\text{S}$ and $\text{Na}_{0.20}\text{Cu}_{1.77}\text{S}$ were synthesized in the melt of a mixture of NaOH and KOH hydroxides at a temperature near 165°C . All reagents (CuCl , NaCl , $\text{Na}_2\text{S} \cdot 9\text{H}_2\text{O}$) were placed in a heated Teflon reactor simultaneously. The nanostructure was formed within 8 hours. The product obtained as a precipitate was washed three times with distilled hot water, and then was washed with pure ethanol. The particle sizes of the resulting powder were in the range from 20 to 400 nm.

X-ray phase analysis was carried out on D8 ADVANCE ECO diffractometer (Bruker, Germany) with the CuK_α radiation. To identify the phases and to study the crystal structure, the software Bruker AXSDIFFRAC.EVA v.4.2 and the

international ICDD PDF-2 database were used.

Images of sample's surface were obtained with using of scanning electron microscope (SEM) MIRA3 from TESCAN.

To check the chemical composition of the samples, an energy-dispersive elemental analysis was performed on the transmission electron microscope Hitachi HT7700 Exalens.

Differential scanning calorimetry and heat capacity (C_p) measurements were performed for solid samples with a DSC404 F1 Pegasus device (NETZSCH, Germany) in an argon atmosphere in the temperature range (300-700) K. The heating rate was 10 K/min.

Electronic conductivities and Seebeck coefficients were measured simultaneously in an argon atmosphere with using of ZEM-3 equipment (Ulvac-Riko, ULVAC Inc., Yokohama, Kanagawa, Japan).

The thermal diffusivity (D) was measured by the laser flash method with LFA 467 HT HyperFlash device (NETZSCH, Selb, Germany) under an argon atmosphere. The thermal conductivity (χ) was calculated as $\chi = \rho DC_p$. The sample densities (ρ) to determine thermal conductivities were measured using the sample's geometry and mass.

Results and Discussion

Figure 1 shows the X-ray diffraction patterns of the studied samples $\text{Na}_{0.15}\text{-Cu}_{1.85}\text{S}$, $\text{Na}_{0.17}\text{Cu}_{1.80}\text{S}$ and $\text{Na}_{0.20}\text{Cu}_{1.77}\text{S}$ at room temperature. The diffractograms reveal the polycrystalline structure of the synthesized samples. Based on the diffractograms obtained using the Rietveld method, the phase composition of the synthesized samples was determined. The contributions of different phases to the structure, caused by the technological processes of their formation, were estimated by determining the volume fraction of the contribution of each phase using the equation:

$$V_{\text{admixture}} = \frac{RI_{\text{phase}}}{I_{\text{admixture}} + RI_{\text{admixture}}}, \quad (1)$$

in which I_{phase} is the average integral intensity of the main phase of the diffraction line with the highest intensity for the main phase, $I_{\text{admixture}}$ is the average integral intensity of the admixture phase, and R is the structural coefficient equal to 1.45. According to the results of the analysis, the samples under study are a mixture of three phases:

$\text{Na}_2\text{Cu}_4\text{S}_3$, the lattice type is monoclinic, space group is $C2/m(12)$; measured lattice parameters are: $a=16.14502$, $b=3.82600$, $c=11.94444 \text{ \AA}$, $\beta=96.206^\circ$ (in $\text{Na}_{0.15}\text{Cu}_{1.85}\text{S}$); $a=16.17351$, $b=3.81325$, $c=11.97957 \text{ \AA}$, $\beta=96.074^\circ$ (in $\text{Na}_{0.17}\text{-Cu}_{1.80}\text{S}$); $a=16.18937$, $b=3.79605$, $c=11.92554 \text{ \AA}$, $\beta=96.432^\circ$ (in $\text{Na}_{0.20}\text{Cu}_{1.77}\text{S}$); in [10] the following values were obtained: $a=15.633 \text{ \AA}$, $b=3.862 \text{ \AA}$, $c=10.332 \text{ \AA}$, $\beta=107.6^\circ$.

Cu_2S is chalcocite, the lattice type is hexagonal, space group is $P6_3/mmc(194)$. Measured lattice parameters are: $a=3.88768 \text{ \AA}$, $c=6.66901 \text{ \AA}$ (in $\text{Na}_{0.15}\text{Cu}_{1.85}\text{S}$);

$a=3.92447 \text{ \AA}$, $c=6.64175 \text{ \AA}$ (in $\text{Na}_{0.17}\text{Cu}_{1.80}\text{S}$); $a=3.91854$, $c=6.72141 \text{ \AA}$ (in $\text{Na}_{0.20}\text{Cu}_{1.77}\text{S}$);

Cu_9S_5 is digenite, the lattice type is rhombohedral, space group is R-3m(166). Measured lattice parameters are: $a=3.92651$, $c=47.72157 \text{ \AA}$ (in $\text{Na}_{0.15}\text{Cu}_{1.85}\text{S}$); $a=3.93655$, $c=48.05133 \text{ \AA}$ (in $\text{Na}_{0.17}\text{Cu}_{1.80}\text{S}$); $a=3.92961$, $c=47.98547 \text{ \AA}$ (in $\text{Na}_{0.20}\text{Cu}_{1.77}\text{S}$).

Table 1 presents the results of estimation of the volume fraction of each phase in the sample structures.

All copper chalcogenides have some homogeneity range with metal deficit, and perhaps on this reason the three observed phases in $\text{Na}_{0.15}\text{Cu}_{1.85}\text{S}$, $\text{Na}_{0.17}\text{Cu}_{1.80}\text{S}$ and $\text{Na}_{0.20}\text{Cu}_{1.77}\text{S}$ samples have different nonstoichiometry degree. The average lattice parameter increases with increasing of metal deficiency in cationic sublattice.

Table 1.

Phase composition of samples (volumetric, %).

Sample Phase	$\text{Na}_2\text{Cu}_4\text{S}_3$	Cu_2S	Cu_9S_5
$\text{Na}_{0.15}\text{Cu}_{1.85}\text{S}$	56.7	35.8	7.5
$\text{Na}_{0.17}\text{Cu}_{1.80}\text{S}$	73.9	14.5	11.6
$\text{Na}_{0.20}\text{Cu}_{1.77}\text{S}$	84.7	6.8	8.5

As can be seen from the Table 1, an increase in the concentration of sodium in the total composition of the mixture leads to an increase in the volumetric contribution of the $\text{Na}_2\text{Cu}_4\text{S}_3$ phase with monoclinic lattice symmetry. Along with this, the volume contributions of chalcocite and digenite phases decreases. The changes in the phase concentrations, obviously, are followed by phase transitions and changes in the main crystallographic characteristics of three phases mentioned above. The hexagonal phase in the pure stoichiometric Cu_2S is observed only above 375 K [13]. The fact that it was found in our samples at room temperature can be explained by the presence of sodium in the lattice, which reduces the temperature of the phase transition from the monoclinic (orthorhombic) to the mid-temperature hexagonal phase.

The increasing of Cu_9S_5 phase concentration in the $\text{Na}_{0.17}\text{Cu}_{1.80}\text{S}$ sample, with a further decrease to 8.5% in the $\text{Na}_{0.20}\text{Cu}_{1.77}\text{S}$ sample is not clear and special study of this fact is necessary.

The difference in the lattice parameters due to the change in the interplanar distances, as well as broadening of the diffraction lines in the diffractograms, may be caused by microstresses in the structure arising as a result of accumulation of dislocations, as well as crushing of crystallites in the crystallization processes. An analysis of the angular dependence of physical broadening makes it possible to estimate the influence of both factors. To assess the effect, the Williamson-Hall method was applied, which is based on the relation [14]:

$$\beta^2 = W_{size}^2 + W_{strain}^2 \quad (2)$$

$$W_{size}^2 = \left(\frac{\lambda}{D \cdot \cos(\theta)} \right)^2, \quad (3)$$

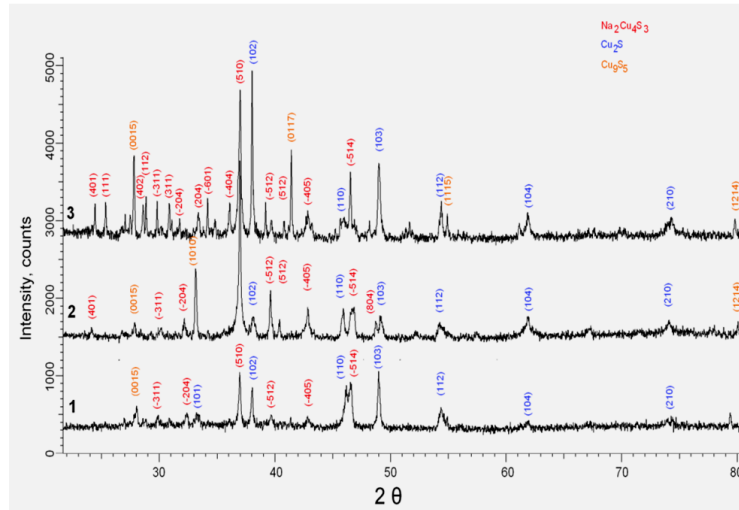


Figure 1. X-ray diffractograms of samples at room temperature: 1) $\text{Na}_{0.15}\text{Cu}_{1.85}\text{S}$; 2) $\text{Na}_{0.17}\text{Cu}_{1.80}\text{S}$; 3) $\text{Na}_{0.20}\text{Cu}_{1.77}\text{S}$.

$$W_{strain}^2 = (4 \cdot \varepsilon \cdot \tan(\theta))^2, \quad (4)$$

where β is a physical broadening of the diffraction maximum, λ is the X-ray wavelength (1.54 \AA), D is the crystallite size, θ is the Bragg diffraction angle, and ε is the value of the microstresses in the lattice.

Assessment of the influence of different contributions with using of (2)-(4) equations shows that broadening of the diffraction peaks is affected both by the deformation and the change in the size of the crystallites. As a result, the change in the parameters of the crystal lattice leads to a change in the lattice volume and, consequently, the density of each phase. The change in the density was estimated using the formula:

$$\rho = \frac{1.6602 \sum AZ}{V_0}, \quad (5)$$

where V_0 is the volume of a unit cell, Z is the number of atoms in a crystalline cell, and A is the atomic weight. Table 2 shows the results of changes in the density of the synthesized samples.

Table 1.

The results of changes in the density.

Sample	Density, g/cm^3		
	$\text{Na}_2\text{Cu}_4\text{S}_3$	Cu_2S	Cu_9S_5
$\text{Na}_{0.15}\text{Cu}_{1.85}$	3.686	6.048	5.718
$\text{Na}_{0.17}\text{Cu}_{1.80}$	3.695	5.989	5.650
$\text{Na}_{0.20}\text{Cu}_{1.77}$	3.707	5.779	5.678

As can be seen from the presented data, an increase in the concentration of the $\text{Na}_2\text{Cu}_4\text{S}_3$ phase in the structure of the synthesized samples leads to an increase in the density of this phase, as a result of which the number of amorphous inclusions and disorder regions decreases in the structure of the samples. One of the important factors affecting the changes in the crystal structure properties and

the defect concentration is the average crystallite size and dislocation density. The dislocation density (δ) contains information on the perfection of the crystal structure and can be estimated from the formula:

$$\delta = \frac{1}{L^2}, \quad (6)$$

where L is the average size of crystallites.

Figure 2 shows changes in the dislocation density in the structure.

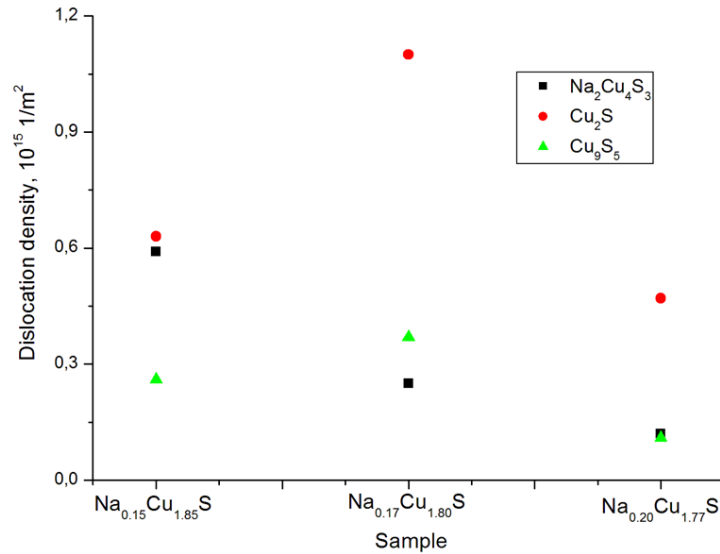


Figure 2. Changes in the dislocation density in the structure.

The density of dislocations of the order of $\approx 10^{15} \text{ m}^{-2}$ is characteristic of strongly deformed crystal lattices [for example, 15]; an increase in the dislocation density in the crystal lattice hampers their motion along the structure, which causes changes in the strength properties and operating characteristics (conductivity, thermal conductivity). At the same time, an increasing in the contribution of the main $\text{Na}_2\text{Cu}_4\text{S}_3$ phase leads to enlargement of the crystallite size and a decrease in the dislocation density for this phase, which indicates an improvement in the crystal structure and a decrease in the number of amorphous inclusions in this phase.

In Figure 3 the SEM images of etched surfaces of $\text{Na}_{0.15}\text{Cu}_{1.85}\text{S}$, $\text{Na}_{0.17}\text{Cu}_{1.80}\text{S}$, $\text{Na}_{0.20}\text{Cu}_{1.77}\text{S}$ samples are shown. The shown particle sizes lies in range about from 30 to 400 nm, a porous structure is observed.

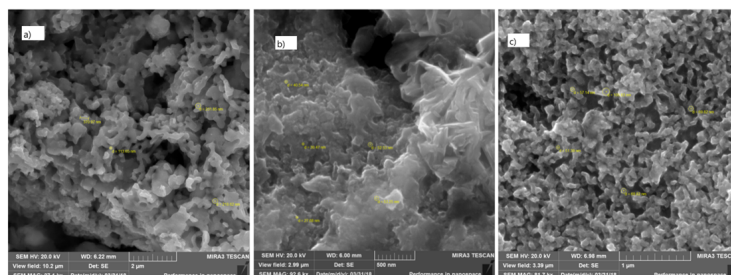


Figure 3. SEM images of etched surfaces of $\text{Na}_{0.15}\text{Cu}_{1.85}\text{S}$ (a), $\text{Na}_{0.17}\text{Cu}_{1.80}\text{S}$ (b), $\text{Na}_{0.20}\text{Cu}_{1.77}\text{S}$ (c) samples.

Figure 4 shows an image of the surface of the $\text{Na}_{0.20}\text{Cu}_{1.77}\text{S}$ sample with a magnification $\times 500$ in the transmission electron microscope Hitachi HT7700 Exalens and the spectrum of the energy-dispersive elemental analysis (E.M.F.) taken for the sample point shown in the photograph.

Unfortunately, sodium radiation is not reliably fixed in the E.M.F. spectra of the samples because of its small ordinal number. On the surface of all samples, a reduced sulfur content is observed, which may be due to its strong volatility. On the porous areas of the surface a significant oxygen content is registered, whereas no oxygen is detected on the smooth surface. No oxygen-containing phases were detected during x-ray phase analysis of the samples, which may indicate only formation of an oxide film on the surface, as the X-ray diffraction method gives a volumetric result, while X-ray spectral analysis uses secondary x-ray radiation from the surface.

Figure 5 shows the results of differential scanning calorimetry and heat capacity (C_p) of the solid $\text{Na}_{0.15}\text{Cu}_{1.85}\text{S}$ sample.

As can be seen from Figure 5, the peak of the DSC signal was detected at 375.6 K with an enthalpy area of $5.234 \mu\text{W}/\text{mg}$, which is close to the data for $\text{K}_{0.1}\text{Cu}_{1.9}\text{S}$ in [6]. The effect arises at about (342 ± 3) K. The thermal effect ends at about 395 K. The heat capacity varies within the range $(0.15\text{-}0.48) \text{ J}/(\text{gK})$.

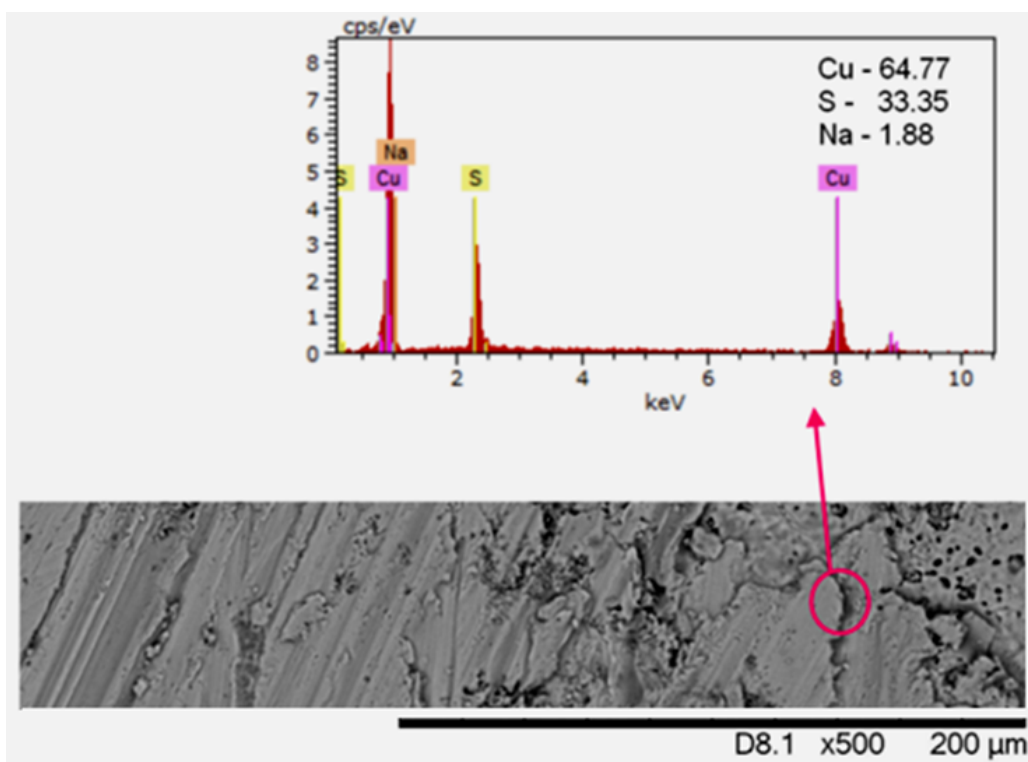


Figure 4. An image of the surface of the $\text{Na}_{0.20}\text{Cu}_{1.77}\text{S}$ sample at $\times 500$ magnification in the transmission electron microscope Hitachi HT7700 Exalens and the E.M.F. spectrum taken for the sample point shown in the photograph.

Among the known phase transitions in the Cu-S system in this temperature region, the transition from the low-temperature phase of jurleite can occur, which, depending on the chemical composition (from $\text{Cu}_{1.934}\text{S}$ to $\text{Cu}_{1.971}\text{S}$), can occur in the temperature range from $(345 \pm 3)\text{K}$ to $(366 \pm 2)\text{K}$. Another possibility is the phase transition from a monoclinic chalcocite Cu_2S to a hexagonal one,

which with copper deficiency (composition $\text{Cu}_{1.993}\text{S}$) can occur at (363 ± 2) K [13] instead of 377 K. At 364 K, a transition also occurs from the low-temperature rhombohedral modification of $\text{Cu}_{1.8}\text{S}$ digenite to the mid-temperature hexagonal modification [13]. Thus, taking into account the results of X-ray phase analysis, we can conclude that the endothermic heat effect in Figure 5 is most likely the result of the phase transition from a rhombohedral digenite to a hexagonal one.

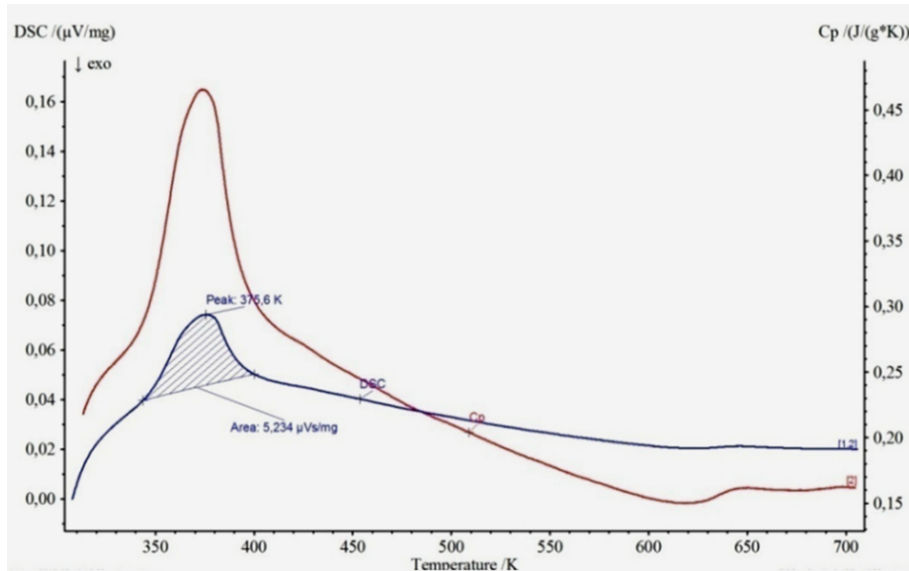


Figure 5. The DSC curves and heat capacities of the solid $\text{Na}_{0.15}\text{Cu}_{1.85}\text{S}$ sample

A shallow minimum on the DSC curves and heat capacity at 625 K in Figure 4 can also be caused by a phase transformation, the nature of which can be clarified by X-ray phase analysis at high temperatures. The phase transition at (370–380) K is accompanied by a sharp jump in the specific heat, which indicates a first-order phase transition. In the series of compositions $\text{Na}_{0.15}\text{Cu}_{1.85}\text{S}$, $\text{Na}_{0.17}\text{Cu}_{1.80}\text{S}$ and $\text{Na}_{0.20}\text{Cu}_{1.77}\text{S}$, the heat capacity at the point of phase transition increases with increasing sodium content. This can be interpreted as an indirect evidence of sodium participation in the formation of the crystal lattice of copper sulfide, as with increasing sodium concentration, energy expenditures on mixing of cations (copper and sodium) should increase. Enthalpy of the transition increases with increasing sodium content in the $\text{Na}_{0.15}\text{Cu}_{1.85}\text{S}$, $\text{Na}_{0.17}\text{Cu}_{1.80}\text{S}$ and $\text{Na}_{0.20}\text{Cu}_{1.77}\text{S}$ chain – (5234, 6923, 11720 J/kgK, respectively).

Figure 6 shows the temperature dependences of the electron conductivity (a), Seebeck coefficient (b), and thermal conductivity (c) of $\text{Na}_{0.15}\text{Cu}_{1.85}\text{S}$, $\text{Na}_{0.17}\text{Cu}_{1.80}\text{S}$, $\text{Na}_{0.20}\text{Cu}_{1.77}\text{S}$ samples. High values of Seebeck coefficient and very low values of thermal conductivity are observed. Low thermal conductivity is associated with high ionic conductivity [9, 12] and with the nanocrystalline state of $\text{Na}_{0.15}\text{Cu}_{1.85}\text{S}$, $\text{Na}_{0.17}\text{Cu}_{1.80}\text{S}$ and $\text{Na}_{0.20}\text{Cu}_{1.77}\text{S}$ samples.

Low thermal conductivity is associated with high ionic conductivity [9, 12] and the nanocrystalline state of the samples. In a recent paper [16], a low thermal conductivity was also observed for nanoplates of copper selenide doped with sodium; however, for our samples the thermal conductivity was several times lower because of the much lower electron component of thermal conductivity.

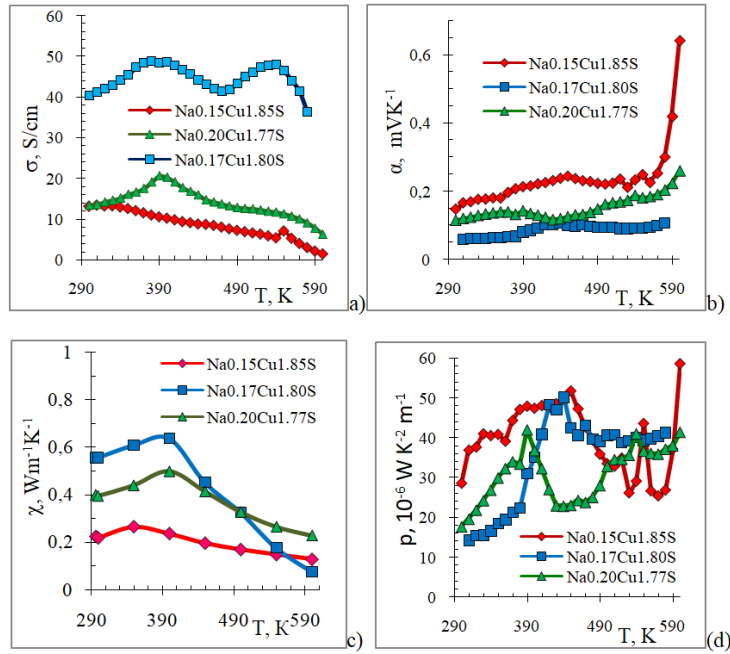


Figure 6. Temperature dependence of the electron conductivity (a), the electronic Seebeck coefficient (b), thermal conductivity (c), and thermoelectric power factor $\rho = \alpha^2\sigma$ (d) of Na_{0.15} Cu_{1.85} S, Na_{0.17} Cu_{1.80} S and Na_{0.20} Cu_{1.77} S samples.

Maximal thermoelectric figure merit $ZT = \alpha^2\sigma T/\chi \approx 0.28$ is observed for Na_{0.15} Cu_{1.85} S at 590 K (Figure 7) and, in our opinion, can be improved by selecting the composition and optimal synthesis conditions.

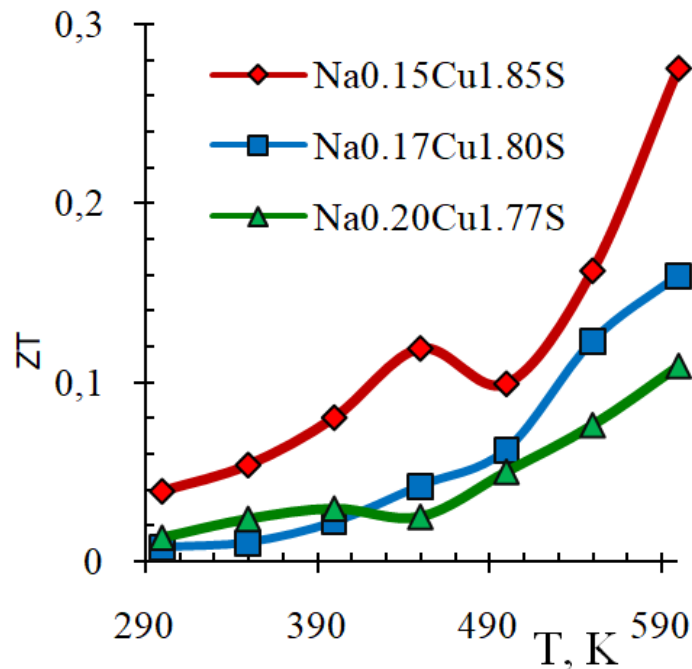


Figure 7. Temperature dependence of the thermoelectric figure merit ZT of Na_{0.15} Cu_{1.85} S, Na_{0.17} Cu_{1.80} S and Na_{0.20} Cu_{1.77} S samples.

Conclusion

In the investigated range of the Na-Cu-S system compositions, the mixtures of three phases are formed at room temperature, -the quasi-one-dimensional monoclinic phase of $\text{Na}_2\text{Cu}_4\text{S}_3$ and two superionic phases - the hexagonal phase of Cu_2S and the cubic phase of Cu_9S_5 . The phase composition of the alloys at high temperatures remains unknown. Apparently, the phase transition observed for all samples at (370-380) K is a transition to a superionic state, an characteristic feature of which is a structural disordering. The structural disordering, "phonon glass" state as well as the small grain sizes, are the factors favoring to the very low thermal conductivity of the samples. Judging from the temperature dependence of the heat capacity for $\text{Na}_{0.15}\text{Cu}_{1.85}\text{S}$, a phase transition should also occur at about 625 K. Unfortunately, the temperature interval of measurements in this study was limited to a temperature of 600 K, and an interesting range of properties above 600 K remained unlighted. In addition to purely scientific interest, the region above 600 K is important for thermoelectric applications, since the thermoelectric efficiency ZT of the alloys increases strongly with temperature increasing. The ZT 0.28 value achieved for the alloys studied is good at 590 K for copper sulfides, but it can be greatly increased, in our view, by lowering the sodium content in non-stoichiometric copper sulfide ($\text{Cu}_{1.75}\text{S} \div \text{Cu}_{1.85}\text{S}$) to the optimum so that the electrical conductivity remains high enough.

Acknowledgments

The authors are grateful to the Ministry of Education and Science of the Kazakhstan Republic for financial support the Program "Development of Hydrogen Energy Technologies in the Republic of Kazakhstan" (2018–2020).

References

- [1] R. Scheer, H.-W. Schock, Chalcogenide Photovoltaics: Physics, Technologies, and Thin Film Devices (WILEY-VCH Verlag&Co, Germany, 2011) 386 p.
- [2] P. Qiu, X. Shi, L. Chen, Energy Storage Materials **3** (2016) 85.
- [3] Y.Q. Tang et al, Crystals **7** (2017) 141.
- [4] M.Kh. Balapanov et al., Inorganic Materials **50** (2014) 930.
- [5] T. Ohtani et al., J. SolidState Chem **115** (1995) 379.
- [6] M.M. Kubenova et al., Actual problems of micro- and nanoelectronics. Collection of V All-Russian scientific youth conference with international participation, Ufa (2018) 232.
- [7] H.T. Evans, Zeitschriftf Ur Krist **150** (1979) 299.
- [8] A. Putnis, Amer Min. **62** (1977) 107.
- [9] R.A. Yakshibaev et al., Fizika tverdogo tela (USSR) **28**(5) (1986) 1566.
- [10] G. Savelsberg, H. Schafer, Mat. Res. Bull. **16** (1981)1291.
- [11] Z.H. Ge et al., Adv. Energy Mater. **6**(16) (2016) 1600607.
- [12] M.K. Balapanov et al., Ionics **24** (2018) 1349.

- [13] D.J. Chakrabarti, D.E. Laughlin, *J. Phase Equilibria* **4**(3) (1983) 254.
- [14] K. Venkateswarlu et al., *Physica B: Condensed Matter* **405** (2010) 4256.
- [15] Xiaolei Wu, En Ma, *Applied Physics Letters* **88**(23) (2006) 231911.
- [16] Yingshi Jin et al., *Appl. Sci.* **8** (2018) 12.